Indian Journal of Engineering & Materials Sciences
Vol. 30, June 2023, pp. 437-446
10.56042/ijems.v30i3.3792

Ion-beam-induced Modifications of Nanocrystalline ZnO thin Films Grown by Atomic Layer Deposition

Deepika Gupta[a], Shweta Sharma[b*], Sonica Upadhyay[c], S K Sharma[d], Vishnu Chauhan[a], & Rajesh Kumar[a]

[a]University School of Basic and Applied Sciences, Guru Gobind Singh Indraprastha University, New Delhi 110 078, India

[b]Department of Botany, Sri Venkateswara College, University of Delhi, New Delhi 110 021, India

[c]Department of Computer Science & Engineering, Maharaja Surajmal Institute of Technology, New Delhi, 110 058, India

[d]University School of Information and Communication Technology, Gautam Buddha University, Greater Noida 201 312, India

Received: 10 May 2023; Accepted: 31 May 2023

Irradiation with distinct ions turns out to be an efficacious way to alter the optical, structural, electrical and morphological properties of different materials by instigating the strains, defects and structural transitions in it. Ion beam irradiation with Swift Heavy Ion (SHI) can originate defects in the materials by conveying the adequate energy to the lattice results into materials modifications. We will extensively study how the SHI irradiation influences the Atomic Layer Deposition (ALD) Grown Zinc Oxide (ZnO) thin films' distinct characteristics, which may be applicable for evolving the distinct sensors, capacitors and optical devices based on it. In the present work, the influence of high electronic energy deposition on the physico-chemical and morphological properties of ZnO thin films synthesized by ALD technique have been investigated at different fluences. The thin films of ZnO irradiated by 120 MeV $Ti^{9+}$with a fluence of 5E11 to 1E13 ions/cm^2. Atomic Force Microscopy (AFM) analysis reveals notable grain boundaries and proposed that the roughness of irradiated thin films alters as compared to pristine thin films. The thickness of ZnO thin films were estimated by Rutherford backscattering spectroscopy (RBS). Photoluminescence (PL) intensity enhancement has been remarked in the Ti ion beam treated ZnO thin films samples as compared to pristine specimen. The alterations of the of Zn 2p and O 1sbinding energy of pristine and ion irradiated thin films were examined by X-ray Photoelectron Spectroscopy (XPS).

Keyword: Atomic Force Microscopy (AFM), Atomic Layer Deposition (ALD), Rutherford Backscattering Spectroscopy (RBS), Swift Heavy Ion (SHI), X-ray Photoelectron Spectroscopy (XPS), Zinc Oxide (ZnO)

1 Introduction

One of the basic challenges in materials science is to identify the real effects of ion beam irradiation on solid surfaces of the materials. Indium Tin Oxide (ITO) is considered to be promising transparent conductive oxide (TCO) material exhibits resistivity in the range of 10^{-4} Wcm^{-1}. On account of the scantiness and high price of indium, there have been numerous efforts to substitute ITO. The most encouraging expectant material is ZnO which is inexpensive[1-2]. ZnO is a prominent n-type semiconductor. ZnO exhibits a firm wurtzite hexagonal structure under ambient conditions. ZnO contains a 60 meV large exciton binding energy value at ambient temperature conditions and a direct bandgap value of 3.37 eV. Exciton binding energy of ZnO is twice greater than the GaN, establish it as one of the efficacious alternatives in the domain of ultraviolet and blue optical devices like ultraviolet laser diodes and light-emitting diodes[3-5]. Even though subjected to fabricating conditions and methods, the photoluminescence considerations disclose the relationship between defects in ZnO films and particular emissions in the visible range[6]. On account of numerous applications of ZnO, there is a noteworthy keenness to comprehend the ZnO optical properties[7-9]. Furthermore, ZnO contains a significant broad visible emission and strong emission in the wavelength range of UV range. In ZnO the origination of emission band in the UV range is related with band-to-band transition and recombination of excitons. The emission found in the visible range is corresponding to the extrinsic or intrinsic defects. Additionally, to photoluminescence, other techniques like EPR (electron paramagnetic resonance) have been explored to verify the behavior of defects accountable for visible luminescence[9-11]. Nanostructures and thin films based on ZnO have been explored for numerous applications like solar

*Corresponding author (E-mail: amu.shweta@gmail.com)

diode sensors, solar cells, TCO (transparent conducting oxide), bulk acoustic wave devices, transistors and ultra-violet light emitters[12-15]. Current progress in ZnO processing has disclosed distinctive applications for phosphors, UV light emitters, varistors, sensors, high-power transparent electronics, optoelectronic devices and piezoelectric transducers[16]. In addition to ZnO in bulk form and thin films, but also ZnO in nano-structured forms like nanoparticles and nanowires has been effectively researched for distinct applications[17]. As the devices based on optoelectronics demands high-quality optical coating along with high packaging density, high surface uniformity, low defect density and exhibits appreciable adhesion with the substrate and regulate the thickness of the film, all these factors rely on the growth method being explored[18].Thin films based on ZnO have been grown by distinct techniques like sol-gel[19], spray pyrolysis[20], sputtering[21], chemical bath deposition, metal-organic chemical vapor deposition, atomic layer deposition, pulsed laser deposition (PLD) and molecular beam epitaxy (MBE)[22]. However, all these techniques demand processing a high value of temperature to acquire adequate electrical properties like low operating voltage and high mobility for applications based on devices, therefore not appropriate for the growth of thin films of ZnO on organic dielectrics and flexible substrates. In recent times ALD method has been distinctly illustrated its efficiency of growing thin films at low-temperature value[23]. ALD technique is appraised as specific mitigation of chemical vapor deposition for self-regulating growth of films[24]. ALD is a technique based on alternating surface-regulated reactions to bring about exceptionally uniform and conformal thin films with the thickness regulation of sub-nanometer accuracy and efficiency in giving rise to thin films of a distinct materials' variety. ALD became a prominent technique for many research and industrial applications on account of above-mentioned advantages of this technique[25-27]. On account of self-regulating surface chemical reactions in the ALD technique, there are three practical ways to regulate the properties of film; (a) process steps of ALD (purge and dose times), (b) alternative of precursors and (c) films' post-processing[27]. ALD reactions exhibit two chemicals, specifically known as precursors which react with the material's surface one after another in a consecutive manner. When the surface of the substrate is unveiled to the precursors frequently, a film with an excellent attribute is attained. ZnO thin films grown by the ALD technique have attracted significant attention in the domain of semiconductor devices on account of their ultra-thin thickness, high purity and crystallinity which affect electrical and optical characteristics of the film and establish it as a significant member of optoelectronics domains. For the origination of nanocrystalline materials swift heavy ion (SHI) irradiation is considered to be unique and efficacious ways. SHI beam irradiation spends energy in the adjacency of the ion path and contributed swiftly to the adjacent lattice. Melting of an area with a radius of few nanometers take place in the ambiance of the target material that comes in the path of ions and the process of recrystallization occurs in the course of dynamic annealing following the origination of well defined nanocrystalline phases[28,29]. In the present experimental work we are intended to utilize beam of high energy Ti^{9+} ion irradiation with fluence ranges from 5E11 to 1E13 ions/cm^2 as a significant route for tailoring the local surface region of ALD grown ZnO thin films specimens to extensively comprehend the optical, physical and morphological characteristics of pristine and ion irradiated ZnO thin films grown by ALD technique.

2 Materials and Methods

2.1 Synthesis

Thin films of ZnO were synthesized on glass and silicon substrate utilizing the Atomic layer deposition technique. For the deposition of thin films of ZnO PicosunSunale^{TM}, ALD system was utilized. The substrate was utilized exhibits a dimension of 1×1 cm^2 to get consistent growth of films. Before deposition, the substrate was washed with deionized water, isopropyl alcohol and acetone. The growth of thin films was done at temperature of 200°C and the rate of deposition during experiment was 0.9 Å/cycle LD was used at high temperature utilizing alternating Zn $(CH_2CH_3)_2$ and H_2O exposures for the growth of ZnO thin films on glass and silicon substrate.

2.2 Interaction of ion and matter

The grown ZnO specimens were treated with 120 MeV Ti^{9+}SHI at a distinct fluence of 5E11, 1E12, 5E12 and 1E13 ions/cm^2. The irradiation experiment was accomplished at Inter-University Accelerator Center (IUAC), New Delhi India[30]. When an ion with high energy interacts with the material moves through

the target material, it eradicates its energy on account of collisions with target atoms and eventually ceases. The manner by which ions lose their energy predominantly commanded by elastic collisions occurs in the regime of low energy (generally up to ~10keV/amu), is associated with nuclear energy loss (S_n). Inelastic collision prevails in regime of high-energy generally energy beyond the ~1MeV/amu is associated with electronic energy loss (S_e). In the regime of electronic energy loss, ions exhibit significantly high energy that the orbital electron velocity of ion is corresponding to or greater than Bohr electron velocity[31,32]. The S_n, S_e, range, longitudinal and lateral straggling values are demonstrated by the SRIM computer codes[33], are found to be 1.286 Å/eV, 1.033×10^3 Å/eV, 14.17µm, 5393 m Å and 5940 m Å respectively. Ions exhibit significant energy varies from few keV to few MeVs strike atoms of the material and partly convey their energy to the material atoms. Additional recoils give rise to collision cascade through the recoiled or displaced atoms with significant energy. The elastic collision of proceeding ions sustains till the ion eventually stops. After Ti ions irradiation on ZnO thin films from SRIM analysis it is found that S_e is predominates over S_n. Therefore, it is anticipated that SHI beam irradiation causes collision cascade.

3 Results and Discussion

3.1 RBS Studies

The quality of ZnO thin films was demonstrated by Rutherford backscattering Spectroscopy (RBS) measurements. RBS spectra studied to evaluate the local surface stoichiometric ratio of thin films of ZnO samples. Thus, 2 MeV of αparticles interact with the samples and then backscattered α particles were collected in the detector of RBS assembly setup gives the counts for the evaluation of surface composition. The composition and thickness estimation were accomplished by RBS analysis[34]. RBS of virgin and Tiion beam irradiated ZnO thin films is represent in Fig 1. RBS spectra are consistent with previous literature reports[35, 36]. Measurements based on RBS have been taken by utilizing 5SDH-1.7MV Tandem accelerator at IUAC, New Delhi. Scattering cross-section is responsible for the RBS signal intensity which is directly associated to the square of the element atomic number[37]. It is remarked that edge related with Si is not so sharp attributed that some intermixing at the interface of Si/ZnO takes place. With respect to direction of incident ion beam perpendicular geometry has been utilized. During RBS measurements chamber has been maintained at high vacuum conditions. The RBS of pristine and Ti ion beam irradiated samples of ZnO thin films were taken with $4He^+$ beam of ion exhibits energy of 2MeV and charge of 12µC was used for each analysis. Fig. 1. Illustrate the RBS spectrum of virgin and Ti^{9+} ion beam irradiated samples with a fluence of 5E11, 1E12, 5E12 and 1E13 ions/cm^2 thin films of ZnO which signifies that the virgin and Ti ion beam irradiated samples of ZnO thin films exhibits nearly same thickness as of pristine thin films of ZnO. RBS spectra fitting are done with the simulation program known as simulation of nuclear reaction analysis (SIMNRA) software. The distinct parameters of films are demonstrated by simulating RBS spectra in SIMNRA software. Detected elements overall concentration provides the details of thin films of ZnO. The surface edge for the distinct elements (Zn and O) can be distinctly remarked [38]. The high channeling yield displayed that thin films of ZnO exhibit intrinsic defects specifically of interstitial in nature. Generally, oxygen vacancies, zinc interstitial and antisite defects were considered to be found in ZnO thin films. The RBS measurements of virgin and Ti ion beam irradiated thin films' samples are identical in nature attributed that very small change occurs in the composition and near surface region of the samples. The RBS spectra plateau region signifies the silicon substrate. The composition in ZnO thin films is found to be Zn (0.36) and oxygen (0.64). The excess oxygen present in the films on account of its

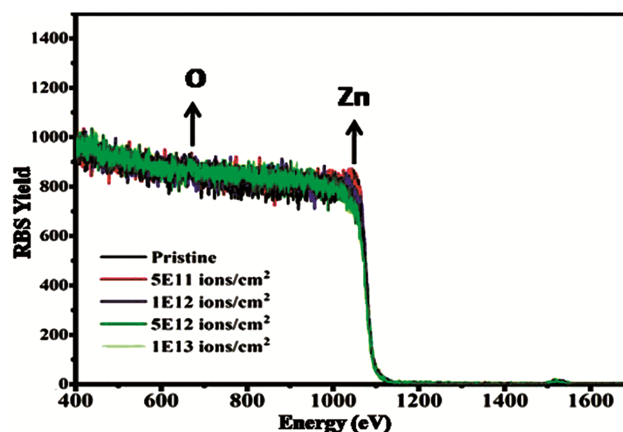

Fig. 1 — Variation of RBS spectra of Pristine and ion treated ZnO thin films samples.

presence in the interfaces between the micro crystallites or grain boundaries. Simulation of experimental data with SIMNRA software displayed that concentration of oxygen is high in contrast to Zn concentration. The thickness of films is found to be approximately 15 nm. As crystalline quality decreases after ion beam irradiation at distinct fluence as indicated by Zn edge sharpness decreases. Thus, crystal structure alteration is anticipated after high energy irradiation of ZnO grown thin films[35]. Specifically, the amount of lattice disorder progressively increases with the enhancement in ion fluence and the irradiated samples display identical RBS spectra. The concentration depth profiles are found to be broadened on account of straggling of ion energy during the ions interaction with specimens; it can be explained on the basis of partial channeling of Ti ions or Ti ions'diffusion in the structure of ZnO. It was studied that minimum energy requires for channeling depend on lattice orientation and instigate distinct ranges of ions that are bombarded for each position of channel. The scattering of ions that is non-channeled into channels results into broadening of species depth profiles during irradiation becoming prominent during irradiation. The resolution of depth in RBS spectra is influenced by irradiated ions' straggling causes' energy loss and energy resolution of detector. Ti is considered to be an element with heavy mass with its energy loss is greater in contrast to target material[36]. Some alterations have been remarked in the peak corresponding to the Zn in RBS spectra. This has been associated with the irradiation instigated micro structural defects like decrease in crystallite size, escalation in dislocation density and may be surface defects[39].

3.2 AFM Study

The morphology of surface of unirradiated and Ti^{9+} ion beam treated thin films with a distinct fluence are examined by AFM as given in Fig 2. During AFM measurements, the AFM was done on silicon substrate with Bruker nanoscopemulti-mode 8 AFM at room temperature in scanasyst mode with following specifications spring constant 0.4 N/m, frequency 70 KHz, silicon tip on nitride lever with thickness of 650 nm. The AFM of pristine specimen represents the existence of distinctively inter-connected grain arrangement with a consistent pattern. The scanned AFM micrographs represents a consistent distribution of grain structure of granular ZnO which is a uniform with a fine quality nanostructure thin film exhibit smooth, pin-hole free and crack-free surface[40,41]. The ZnO thin films grown by ALD technique comprises of numerous granular particles with well-ordered sizes. R_a is the average roughness it is defined as mean height as determined over the calculated area/length. It is found to be (0.63, 1.20, 0.69 and 0.77) for virgin and ion treated ZnO thin films R_q is considered to be root mean square roughness (RMS)

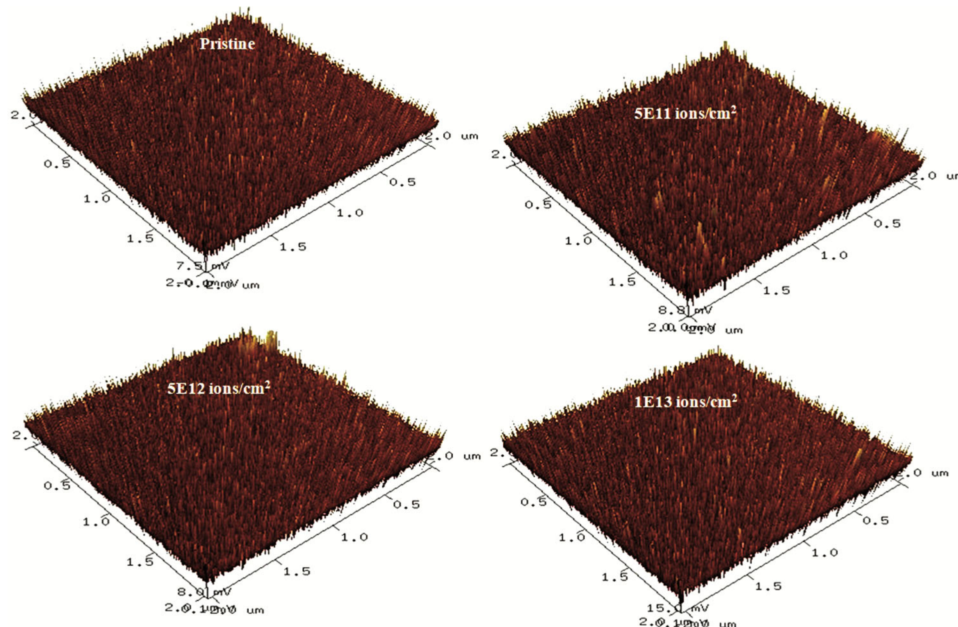

Fig. 2 — 3D AFM image derived for the unirradiated and ion treated ZnO thin films grown by ALD technique.

is the square root of the height of surface distribution and is appraised to be more susceptible as compared to the roughness with average values for deviations from the mean line or plane. It is found to be (0.717, 1.354, 0.785 and 0.871) for unirradiated and ion treated thin films samples.

R_q (root mean square) roughness is calculated by following equation.

$$R_q = \left(\frac{1}{L}\left|\int_0^L \left|(y(x))^2\right|.dx\right)^{1/2} \quad \ldots (1)$$

Where L represents the profile length utilized for the measurement at x-axis and y(x) is the alteration of the height from the line of profile for data points.

Roughness results reveal that there is slight change in R_a and R_q of ZnO thin films after Ti^{9+} ion beam irradiation. The grain size was calculated with Gwyddion software. Software based on Gwyddion used to study z difference between two points considered in probing the grain size. The average gain size is studied using Gaussian height distribution from 2D image for the unirradiated and ion treated samples[42]. It is calculated to be (31.8, 27.6, 31.2 and 37.4 nm) for unirradiated and ion treated thin films. Grain size also alters with the ion beam irradiation, small reduction in grain size is remarked after ion beam treatment with 5E11 and 5E12 ions/cm^2 fluence, and then at higher fluence increment in grain size is inferred. When swift heavy ions interact with the target material, conveys a noteworthy amount of energy in to the material. On account of energy deposition by energetic ions leads to the alteration in film surface. The grain size decreases after ion beam irradiation with low fluence of 5E11 ions/cm^2 on account of origination of internal strain caused by SHI bombardment. Decrease in size of grain also remarked because of diffusion of surface phenomenon by the influence of high energy ions[43]. There is a significant alteration remarked in the values of the R_a and R_q corresponding to the films irradiated with the fluence of 5E11 ions/cm^2, and with the enhancement in ion fluence the roughness values decreases. Reduction in grain size occurs on account of particles fragmentation in films irradiated with Ti ion beam, such alterations is ascribed to creation of electronic excitation with high density on account of swift heavy ion irradiation under the influence numerous impacts near the ZnO thin films surface. The enhancement in roughness values from 0.717 to 1.354 occurs due to origination of corrugation of surface through heating occurred by ion beam irradiation and decreases in roughness at higher value of Ti ion beam fluence on account of ion tracks' overlapping, bring about diffusion of volume in thin films of ZnO. Thus, escalation in roughness values of ZnO thin films at 5E11 ions/cm^2 fluence may be due to formation of electron cascade and defects formation by Ti^{9+} ions on the surface of ZnO thin films[44, 45].

3.3 XRD Study

The XRD pattern of unirradiated and ion treated ZnO thin films at distinct fluence value of 5E11, 1E12, 5E12, 1E13 ions/cm^2 is given in the Fig. 3. In virgin sample the peak is studied parallel to the plane (101)[46]**.** XRD pattern of pristine sample displays ZnO sharp peak, which signifies the crystallinity nature of thin films of ZnO by ALD technique. These results are consistent with the JCPDS card no 36-1451. The parameters of crystal structure of pristine sample like size of crystallite (D), density of dislocation (d), micro strain(ε) and interplanar spacing (L) are calculated by following equations

$$D = \frac{K\lambda}{\beta\cos(\theta)} \quad \ldots (2)$$

$$\varepsilon = \frac{\beta\cos(\theta)}{4} \quad \ldots (3)$$

$$d = \frac{1}{D^2} \quad \ldots (4)$$

$$L = \frac{\lambda}{2\sin(\theta)} \quad \ldots (5)$$

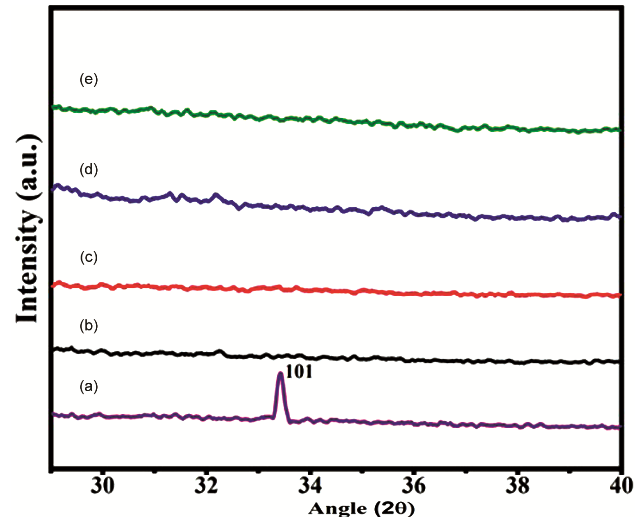

Fig. 3 — (a) XRD of pristine and (b-e) sample irradiated with Ti ions with distinct fluence (5E11 to 1E13 ions/cm^2).

λ represents the of X-ray wave length, θ gives a value of Bragg angle, β represent FWHM in radians[47]. The crystallite size (D), density of dislocation (d), micro strain(ε) and interplanar spacing (L) parallel the plane (101) are found to be 51nm, $0.066\times10^{16}m^{-2}$, 0.384×10^{-3} and 2.67 A° respectively. With the Ti ion beam treatment of thin films, the amorphization of thin films remarked. ZnO films amorphization can be illustrated on the accordance of origination of latent tracks. Thus origination of amorphous latent tracks will occur[48]. Shock waves are generated by these latent tacks give raise to radial pressure adjacent the tracks, which leads to perpetual disorder in the system. The origination of these latent tracks can be illustrated in accordance with model based on thermal spike. This model illustrate that when the energetic ions interaction takes place with the material, the ejected electron kinetic energy is conveyed to the materials' lattice structure through electron-phonon reciprocity in a prominent manner to enhance the temperature of the lattice above the material melting point. This enhancement in temperature leads to quick thermal quenching (10^{-13}K/s) that bring about columnar structure, when the solidification of melted material occurs[49].

3.4 XPS Study

XPS measurements were taken with radiation source of Alk$_{\alpha}$ with hν is equal to 1486.7 eV with vacuum level of 5.2×10^{-10} mbar. The angle between analyzer and source is set at 90°, with analyzer resolution is 0.60 eV. Survey spectra of ALD grown virgin and ion beam treated samples are given in Fig 4. Table 1 encapsulates the value of binding energy and FWHM of Zn 2p, C 1s and O 1s of virgin and ion treated sample with distinct fluence (5E11 and 1E13 ions/cm^2). The weak carbon peak centered at 283 eV is remarked in fig. 4a, on account of thin films exposure to environment before the XPS measurement and intensity of C1s peak increases after ion beam treatment with a fluence value of 5E11 and 1E13 ions/cm^2. Peak ascribed to 3d, 3p, 3s Zn core levels are also remarked. In pristine sample, Zn peaks centered at 1022.7 and 1045.8 eV can be attributed to the Zn 2p doublet (Zn $2p_{3/2}$ and Zn $2p_{1/2}$) sequentially. Calculated difference between two peaks is found to be 23.1 eV, which is consistent with the Zn^{2+} bound with O binding energy. The peak at 1022.7 is sharp in nature signifies that species of Zn, exist in films are thoroughly in oxidized state. In sample treated with 5E11 ions/cm^2, Zn 2p doublet is remarked at 1022.6 and 1045.9 eV in fig. 4b. In the sample irradiated with a fluence of 1E13 ions/cm^2 Zn2p doublet is remarked at 1022.96 and 1046.11. The binding energy value of Zn 2pdoublet shift towards higher binding energy values after the ion beam treatment with higher fluence value of 1E13 ions/cm^2. This shift in binding energy of 0.31 and 0.26 eV parallel to the Zn 2p doublet in the sample treated with the 1E13 ions/cm^2 signifies that reduction in valence electron density occurs and enhances the oxidation state[50]. The intensity of peaks corresponding to the Zn 2p doublet slightly reduces after ion beam treatment of specimens irradiated with 5E11 ions/cm^2 and great escalation in peaks' intensity is observed for the samples treated with fluence value of 1E13 ions/cm^2. The O1s core level is remarked at 532.6 eV, 532.4, 532.5 for pristine and ion treated samples in fig 4c. The binding energy of O1s decreases after ion beam treatment with a fluence value of 5E11 and 1E13 ions/cm^2. Intensity parallel to O1s core level decreases after ion beam treatment with a fluence

Table 1 — Pristine and ion irradiated samples' survey spectra and binding energy value of core level region and FWHM value

Core Levels	Pristine		5E11 ions/cm^2		1E13 ions/cm^2	
	Binding Energy (eV)	FWHM	Binding Energy (eV)	FWHM	Binding Energy (eV)	FWHM
O 1s	532.00	1.741	532.00	1.77	532.00	1.85
C 1s	283.50	1.550	283.50	2.00	283.50	2.32
Zn 2p	1022.5	2.630	1022.0	2.00	1023.5	2.21

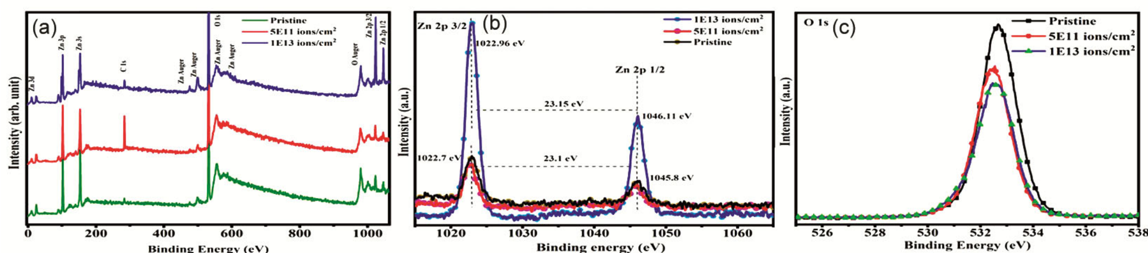

Fig. 4 — (a) Survey spectra, (b) Zn 2p XPS, (c) O 1s XPS spectra of virgin and ion treated ZnO thin films specimens.

value of 5E11 and 1E13 ions/cm^2. It is concluded that the peak intensity is associated with alterations in the oxygen vacancies concentration. Thus, alterations in the O1s component intensity may be associated relatively to the oxygen vacancies concentration [51].

3.5 Photoluminescence (PL) Study

Photoluminescence is a non-destructive technique explored for evaluation of structure of defects in ZnO thin films on glass substrate. ZnO is a important luminescent material contains mainly two bands of luminescence first region is 3.1-3.3 eV, on account of exciton, second region is present in the range of 1.8-2.4 eV on account of defects. The luminescence associated with excitons exhibits a lifetime less than 1 ns in thin films of ZnO, thus it is feasible to derive a fast scintillator[52]. Photoluminescence study of thin films specimens reveal the emissions near the ultraviolet (UV), blue, red and green. Although, in ZnO thin films' PL spectra the center of recombination and mechanisms responsible for the explanation of these emissions are not very clear. ZnO luminescence is very susceptible to the state of the surface and regulated by the method of synthesis. Also the type of substrate also affects the ZnO luminescence. As the previously reported findings suggested that heavy ions with high energy causes the electronic energy loss leads to oxygen desorption from the target material surface, which enhances with escalation in ion dose [53]. Fig. 5a. represents the PL spectra of ZnO thin films in 320-500 nm range of wavelength at 270 nm excitation wave length. In fig 5a. PL emission peaks is remarked at the 328nm (3.78 eV), 342nm (3.62 eV), 377nm (3.28eV), 396 nm (3.13 eV (UV)), 406 nm (3.05nm (violet)), 438 nm (2.83 eV (blue)), 458nm (2.707 eV (blue)), 468nm (2.64eV (blue)), 478nm (2.59 eV (blue-green)) wavelength. Study of PL spectra measurements can be classified in two bands of luminescence (1) emission band exist in visible range of spectra exhibits a range of (400-630 nm), (2) emission band present in (UV) range of spectra exists at the wavelength of 394 eV. Emission band associated with visible region is related with defects signifies deep-level emissions[54] and UV emission is present on account of near-band emission (NBE)because of transition of electrons takes place from the conduction band to valence band[55]. Generally, ZnO mainly exhibits six types of bands, like interstitials of oxygen(O_i), vacancy of oxygen (V_O), vacancy of Zinc (V_{Zn}), oxygen antisite (Zn_O), antisiteof Zinc (O_{Zn}) and Zinc interstitials (Zn_i). The spectra present in visible range mainly exhibits violet, blue, green, yellow, blur green and yellow-green emissions. The peaks of emission associated with the emission related with the deep-level is evaluative issue, often deep level emission emanates on account of Zn_i and V_O. Wide range of visible spectrum is covered by deep level emission in ZnO films. Concentration of defects decides the intensity of deep level emission. Mainly green emission emanates in ZnO on account of oxygen interstitials, oxygen vacancy[55].In the present work; emission peaks are associated with the UV and visible emission. Peak remarked at 377 nm emanates on account of recombination of free excitons by collision process of exciton-exciton parallel to NBE exciton ZnO emission wide bandgap[55]. The UV emission peaks are also centered at 328, 342,377, 396 nm were remarked for the thin films of ZnO. The peak centered at the position of 438 nm with the energy level of 2.83 eV is associated with emission on account of defects. The interval of energy i.e. 2.83 eV parallel to the emission from defects i.e. adjacent to the donor level, emission corresponding with the energy of 2.9 eV emanates from interstitials of Zn (Zn_i), accordance full-potential linear muffin-tin

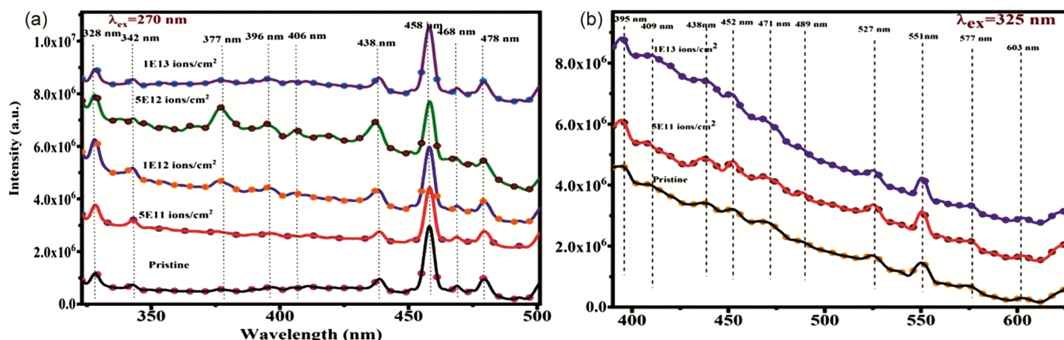

Fig. 5 — (a) PL spectra of virgin and ion treated thin films of ZnO with distinct value of fluence at excitation wavelength of 270nm and 11 (b). PL spectra of virgin and ion treated ZnO thin films with distinct fluence value measured at excitation wavelength 325nm.

orbital method[56]. Thus, blue emission centered at 438 nm may be instigated from electronic transition between the valence band and donor level of Zn interstitial. The blue emission peak present at the wavelength of 458 nm is associated with transition takes place from singly ionized and neutral Zn interstitial levels to the valence band[57]. The emission at wavelength of 468 nm is considered to be blue-green emission may be related with the transition takes place from bottom level conduction band to singly ionized Zn vacancy. A peak centered at 478 nm (2.59 eV) parallel to the blue emission and it represents a deep level visible emission that is associated to the existence of localized levels in energy of bandgap. Although peak centered at wavelength of 478 nm related with the transition from Zn interstitial level to Zn neutral vacancy level. Also the variation of PL spectra is remarked for the excitation wavelength of 325nm in range of the wavelength 389-627 nm. In fig. 5b PL spectra recorded at 325 nm excitation wavelength provides the emission peaks found at the 395 nm (UV), 409 nm (3.03 (Violet)), 438nm (2.83 eV (blue)), 452 nm (2.74 eV (blue), 471 nm (2.61 eV (blue)), 489nm (2.53 eV) (blue-green), 527 nm (2.35 eV (green)), 551nm (2.25 eV (green)), 577 nm (2.14 eV (green)) and 603 nm (2.05 eV (yellow). As intensity of these peaks are not so high on account of more oxygen content present in the films as also studied by RBS composition analysis. As compared to structural and morphological characteristics, the PL was strongly influenced by small alterations occurs in defects density which has strong impact on recombination rates in semiconductor materials [58]. Remarked peaks emission falls in UV, blue and green region of the spectra. Furthermore, parallel to the band-to-band emission, zinc interstitial and oxygen vacancy. The violet emission is generally emanating on account of electrons' transition from conduction band edge to the vacancy level of Zn[59]. The emission of blue band could be originated by the transition of electron from the zinc interstitials and the shallow donor level of vacancies of oxygen to valence band. UV band exists around 396 nm may be associated to the free exciton recombination i. erelated with the NBE (near band edge emission)[60]. The emission peak situated at 409 nm is on account of electrons' transition from the conduction band bottom to interstitials of zinc (Zn_i) level[61]. The emission peaks situated at 438nm, 452nm, 471nm is parallel to the blue emission is related with transition takes place from singly ionized Zn interstitials (Zn_i^+) to the valence band top level. The emission peak corresponding to the 471 nm and 489 nm owing to recombination of conduction band's electrons with the holes present at ionized single vacancy of zinc (V^-_{Zn}).The green emission peak situated at 547nm is attributed to the oxygen interstitial We found that after the Ti ion beam treatment of films, the intensity of UV emission enhances, enhancement in PL emission distinctly remarked in the fluence value of 1E12 ions/cm^2 at 270nm excitation wavelength, then reduces after the ion fluence value of 5E12 ions/cm^2, in the spectra of PL recorded at the 325nmexcitation wavelength, the enhancement in UV emission is found after the fluence value of 5E11 ions/cm^2 and 1E13 ions/cm^2. The increase in intensity of UV PL emission is attributed to the enhancement in the quality of crystal[62]. In the PL spectra excited at a wavelength of 325nm distinctly shows enhancement in the PL intensity of peaks centered at a position of 527nm and 551nm corresponding to the green emission. For the PL green emission defects of Zinc or vacancy of oxygen is mainly responsible. Ion beam irradiation caused the defects associated with vacancies of oxygen. Therefore, luminescence associated with green emission is attributed to the vacancy of oxygen, and enhancement in intensity of green emission recorded at the 325 nm excitation wavelength, signifies that with rise in value of ion fluence give rise to concentration of oxygen vacancies. Himanshi *et al.*[15] reported the enhancement in the green emission when Ga doped ZnO irradiated with the Ag ions with 1E13 and 5E13 ions/cm^2 fluence value. In PL spectra excited at the wavelength of 270 nm of irradiated sample, the peaks corresponding to the 377nm, 396nm, 406nm and spectra recorded at the 325nm excitation wavelength the peaks corresponding to the 409nm, 438nm reduces at high fluence of 1E13 ions/cm^2, it may found because of antisite oxygen depletion from the sample [63].

4 Conclusion

ALD grown thin films of ZnO were irradiated by 120 MeV of Ti^{9+} ion beam with a fluence of 5E11 to 1E13 ions/cm^2 to examine effect of originated alterations in chemical, optical and morphological peculiarities of thin films specimens. The treatment of materials with ions with high value of energy origination of numerous varieties of defects' states in

the system of material occurs, which modify the physical as well as chemical properties like optical, electrical, structural and morphological characteristics of target materials. RBS spectra determined for pristine and ion treated thin films confirms the presence of Zn and O. Pristine and ion irradiated thin films of ZnO exhibit the thickness of 15 nm found by fitting of RBS spectra through software of SIMNRA. Grain size reduction is remarked from 31.8 to 27.6 nm under the influence of ion beam with a 5E11 ions/cm^2 fluence. PL intensity reduction is associated with the formation of defects caused by 120 MeV Ti ion beam after some value of fluence. The binding energy of Zn 2p doublet shift towards higher value binding energy after treatment with ions of higher fluence of 1E13 ions/cm^2. Intensity parallel to the O1s core level decreases after ion beam treatment with a value of fluence of 5E11 and 1E13 ions/cm^2.

Acknowledgments

Prof. Rajesh Kumar acknowledges the Faculty Research Grant Scheme (FRGS) project by Guru Gobind Singh Indraprastha University, New Delhi, India and Inter University Accelerator Center (IUAC), New Delhi, India for project (Ref: IUAC/XIII.3A/ 68308/2020). Prof. R. Kumar is thanks to Prof. N. Koratkar for giving Atomic Layer Deposition (ALD) facility at Rensselaer Polytechnic Institute (RPI), New York, USA. Miss. Deepika Gupta (Ph.D. Scholar) is grateful to Guru Gobind Singh Indraprastha University, New Delhi, India, for giving the Short-Term Research Fellowship (STRF).

References

1 Kim DH, Park MR, Lee GH.. Surface and coatings technology. 201 (2006) 927.
2 Suzuki Y, Niino F, Katoh K. Journal of Non-Crystalline Solids, 218 (1997) 30.
3 Alivisatos AP. Semiconductor clusters, nanocrystals, and quantum dots. science. 271 (1996) 933.
4 Aw K, Tsakadze Z, Lohani A, Mhaisalkar S. Scripta Materialia 60 (2009) 48.
5 Ryu, Y., Lee, T.S., Lubguban, J.A., White, H.W., Kim, B.J., Park, Y.S., Youn, C.J., Applied Physics Letters 88 (2006).
6 Chang YM, Jian SR, Lee HY, Lin CM, Juang JY. Nanotechnology. 21 (2010) 385705.
7 Prakash H, Chandra N, Prakash R.. Journal of Physics B: Atomic, Molecular and Optical Physics. 40 (2007) 1613.
8 Vanheusden K, Seager C. W. t. Warren, D. Tallant and J. Voigt. Appl. Phys. Lett. 68 (1996) 403.
9 Studenikin SA, Golego N, Cocivera M. Journal of Applied physics. 84 (1998) 2287.
10 Repp S, Erdem E. Spectrochimica Acta Part A: Molecular and Biomolecular Spectroscopy. 152 (2016) 637.
11 Gupta, H., Joshi, K., Gautam, S.K., Singh, R.G., Singh, F., Vacuum (2020) 109598.
12 Tang ZK, Wong GK, Yu P, Kawasaki M, Ohtomo A, Koinuma H, Segawa YJ. Applied physics letters. 72 (1998) 3270.
13 Gorla CR, Emanetoglu NW, Liang S, Mayo WE, Lu Y, Wraback M, Shen H. Journal of Applied Physics. 85 (1999) 2595.
14 Wang Y, Sun XW, Goh GK, Demir HV, Yu HY. IEEE Transactions on Electron Devices. 58 (2010) 480.
15 Gupta H, Singh J, Dutt RN, Ojha S, Kar S, Kumar R, Reddy VR, Singh F. Physical Chemistry Chemical Physics. 21 (2019) 15019 .
16 Pearton SJ, Heo WH, Ivill M, Norton DP, Steiner T. Semiconductor Science and Technology. 19 (2004) R59.
17 Gao W, Li Z. International journal of nanotechnology. 6 (2009) 245.
18 Iqbal J, Jilani A, Hassan PZ, Rafique S, Jafer R, Alghamdi AA. Journal of King Saud University-Science. 28 (2016) 347.
19 Zhang Y, Zhang Z, Lin B, Fu Z, Xu J. The Journal of Physical Chemistry B. 109 (2005) 19200.
20 Studenikin SA, Golego N, CociveraM.. Journal of Applied physics. 84 (1998) 2287.
21 Carcia PF, McLean RS, Reilly MH, Nunes Jr G. Applied Physics Letters. 82 (2003) 111.
22 Shan FK, Shin BC, Jang SW, Yu YS. Journal of the European Ceramic Society. 24 (2004) 1015.
23 Motamedi P, Cadien K. Journal of Crystal Growth. 421 (2015) 45.
24 Min YS, An CJ, Kim SK, Song JW, Hwang CS. Bulletin of the Korean Chemical Society. 31 (2010) 2503.
25 George SM. Chemical reviews. 110 (2010) 111.
26 Szilágyi IM, Nagy D. R Journal of Physics: Conference Series 2014 Nov 24 (Vol. 559, No. 1, p. 012010). IOP Publishing.
27 Mani GK, Rayappan JB. Superlattices and Microstructures. 67 (2014) 82.
28 Dunlop A, Jaskierowicz G, Rizza G, Kopcewicz M. Physical review letters. 90 (2003) 015503.
29 Chauhan V, Kumar R, Superlattices and Microstructures. 141 (2020) 106389.
30 Agarwal DC, Chauhan RS, Avasthi DK, Khan SA, Kabiraj D, Sulania I. Journal of Applied Physics. 104 (2008) 024304.
31 Mallick P, Rath C, Prakash J, Mishra DK, Choudhary RJ, Phase DM, Tripathi A, Avasthi DK, Kanjilal D, Mishra NC. Nuclear Instruments and Methods in Physics Research Section B: Beam Interactions with Materials and Atoms. 268 (2010) 1613.
32 Chauhan V, Kumar R. Materials Chemistry and Physics. 240 (2020) 122127.
33 Kumar V, Gupta R, Ram J, Singh P, Kumar V, Sharma SK, Katiyar RS, Kumar R. Vacuum. 166 (2019) 323.
34 Mbamara US, Olofinjana B, Ajayi OO, Lorenzo-Martin C, Obiajunwa EI, Ajayi EO. Engineering Science and Technology, an International Journal. 19 (2016) 956.
35 Giri PK, Kumari S, Goswami DK. Applied surface science. 256 (2009) 384.
36 Macková A, Malinský P, Jagerová A, Mikšová R, Nekvindová P, Cajzl J, Böttger R, Akhmadaliev S. Vacuum. 169 (2019) 108892.

37 Kwon S, Park HW, Chung KB. Journal of Electronic Materials. 46 (2017) 1210.
38 Monteiro T, Soares MJ, Neves A, Oliveira M, Rita E, Wahl U, Alves E. physica status solidi (c). (2004) 254.
39 Gupta GK, Saini L, Ojha S, Tripathi B, Avasthi DK, Dixit A. Vacuum. 176 (2020) 109342.
40 Perumal V, Hashim U, Gopinath SC, Haarindraprasad R, Liu WW, Poopalan P, Balakrishnan SR, Thivina V, Ruslinda AR. PLoS One. 10 (2015) 0144964.
41 Foo KL, Kashif M, Hashim U, Liu WWCeramics International. 40 (2014) 753.
42 Kumar R, Chauhan V, Koratkar N, Kumar S, Sharma A, Chae KH, Won SO. Journal of Alloys and Compounds. 831 (2020) 154698.
43 Kumar V, Jain A, Pratap D, Agarwal DC, Tripathi A, Chauhan RS. Radiation Effects and Defects in Solids. 168 (2013) 490.
44 Faraz SM, Tajwar Z, Ul Wahab Q, Ulyashin A, Yakimova R. Acta Physica Polonica, A.141 (2022).
45 Kumar V, Singh SK, Sharma H, Kumar S, Banerjee MK, Vij A. Physica B: Condensed Matter. 552 (2019) 221.
46 Hasnidawani JN, Azlina HN, Norita H, Bonnia NN, Ratim S, Ali ES. Procedia Chemistry. 19 (2016) 211.
47 Rathika R, Kovendhan M, Joseph DP, Pachaiappan R, Kumar AS, Vijayarangamuthu K, Venkateswaran C, Asokan K, Jeyakumar SJ. Nuclear Engineering and Technology. 52 (2020) 2585.
48 Studer F, Houpert C, Groult D, Fan JY, Meftah A, Toulemonde M. Nuclear Instruments and Methods in Physics Research Section B: Beam Interactions with Materials and Atoms. 82 (1993) 91.
49 Dixit G, Singh JP, Srivastava RC, Agrawal HM. Nuclear Instruments and Methods in Physics Research Section B: Beam Interactions with Materials and Atoms. 269 (2011) 133.
50 Nakamura A, Temmyo J. Journal of Applied Physics. 109 (2011) 093517.
51 Kumar V, Kumar V, Som S, Purohit LP, Ntwaeaborwa OM, Swart HC. Journal of alloys and compounds. 594 (2014) 32.
52 Tai WP, Oh JH. Journal of Materials Science: Materials in Electronics. 13 (2002) 391.
53 Singh F, Singh RG, Kumar V, Khan SA, Pivin JC. Journal of Applied Physics. 15 (2011) 083520.
54 Fang L, Liu J, Ju S, Zheng F, Dong W, Shen M. Applied Physics Letters. 97 (2010) 242501.
55 Alves E, Rita E, Wahl U, Correia JG, Monteiro T, Soares J, Boemare C Nuclear Instruments and Methods in Physics Research Section B: Beam Interactions with Materials and Atoms. 206 (2003) 1047.
56 Lin B, Fu Z, Jia Y. Erratum, Appl. Phys. Lett. Applied Physics Letters. 100 (2012) 943.
57 Mishra SK, Bayan S, Chakraborty P, Srivastava RK. Applied Physics A. 115 (2014) 1193.
58 Marin O, Tirado M, Budini N, Mosquera E, Figueroa C, Comedi D. Materials Science in Semiconductor Processing. 56 (2016) 59.
59 Chen S, Zhao Z, Tang BZ, Kwok HS. Growth methods, Organic Electronics. 13 (2012) 1996..
60 Kumar K, Valanarasu S, Kathalingam A, Ganesh V, Shkir M, AlFaify S, Applied Physics A. 123 (2017) 1.
61 Farooqi MM, Srivastava RK. Optik. 127 (2016) 3991.
62 Kabir A, Bouanane I, Boulainine D, Zerkout S, Schmerber G, Boudjema B. Silicon. 11 (2019) 837.
63 Kumar PR, Kartha CS, Vijayakumar KP, Singh F, Avasthi DK, Abe T, Kashiwaba Y, Okram GS, Kumar M, Kumar S. Journal of applied physics 97 (2005) 013509.